Article:

Ramirez-Villegas, J and Challinor, AJ orcid.org/0000-0002-8551-6617 (2016) Towards a genotypic adaptation strategy for Indian groundnut cultivation using an ensemble of crop simulations. Climatic Change, 138 (1). pp. 223-238. ISSN 0165-0009

https://doi.org/10.1007/s10584-016-1717-y

Supplementary Information

Towards a genotypic adaptation strategy for Indian groundnut cultivation using an ensemble of crop simulations

Julian Ramirez-Villegas and Andrew J. Challinor

Contents:

SI Text 1: Parameterisation of CO_2 response

Groundnut is a grain legume featuring a C3 photosynthesis pathway (Seeni and Gnanam 1982). Physiologically, therefore, the effects of increase in atmospheric CO_2 concentrations have a direct impact on the production of assimilate (Schmidt et al. 2006; Leakey et al. 2009). Under climate change scenarios of increased CO_2 concentrations, C3 crops are expected to increase their rate of photosynthesis (Chen and Sung 1990; Long et al. 2006; Leakey et al. 2009). The additional production of assimilate is expected to increase water use efficiency, leaf area index, biomass, specific leaf area, radiation use efficiency (*RUE*) and the harvest index (Tubiello and Ewert 2002). As a result, crop yields in C3 crops are expected to increase with increased CO_2 concentrations (Vara Prasad et al. 2003; Challinor and Wheeler 2008a). The parameterisation of CO_2 response in GLAM is thus important for assessing crop growth CO2 stimulation and its combined effect with high temperature or drought stress on reproductive plant processes (i.e. flowering and grain filling) (Clifford et al. 2000; Vara Prasad et al. 2003).

The CO_2 response of the crop was parameterised after Challinor and Wheeler (2008a) (CW2008 hereafter). The methodology developed by CW2008 mainly consisted of perturbing certain crop model parameters to enhance biomass production while increasing water use efficiency. They also introduced a factor (T_{fac}) that controls the response of the normalised transpiration efficiency to varying humidity levels (also see CW2008). Specifically, they introduced changes to the baseline values of the maximum rate of transpiration (T_{Tmax}), transpiration efficiency (E_T) and specific leaf area (SLA_{max}) in order to account for the increased production of assimilate at higher-than-normal CO_2 concentrations using an 18-member model ensemble. In the study of CW2008, first, the baseline value of T_{Tmax} (physiologically limited transpiration rate) was reduced by 17 % owing to the expected reduction in transpiration (Stanciel et al. 2000). To reflect increased biomass production they increased the value of E_T (increases of either 24 % or 40 % were used). They also used two values of T_{fac} (0 and 0.4) to quantify uncertainty in the differential response to high and low VPD (vapour pressure deficit) conditions. Finally, they reduced the baseline value of SLA_{max} by 10 %. Similar approaches to CO_2 stimulation are used in other crop models, where either the radiation use efficiency (Jones et al. 2003) or the transpiration efficiency (Keating et al. 2003) are increased to reflect increases in net photosynthesis.

In this study, the same four GLAM parameters were changed, but the factors differed (Table S1). This was because the factors employed by CW2008 were defined for doubled CO_2 conditions (350 ppm x 2 = 700 ppm). Scaling was thus needed for 2030s climate as used here. For the concentrations projected by 2030s in RCP4.5 (450 ppm) these four consisted in moderate (+8.8 %) and large (+14.7 %) increases in transpiration efficiency in combination with a decrease of 6.2 % in physiologically limited transpiration (T_{Tmax}), a decrease of 3.7 % in specific leaf area (SLA_{max}), and a moderate and low sensitivity of the crop to CO_2 enhancement under low VPD conditions (T_{fac}). Genotypic adaptation perturbations were in all cases applied over the CO_2-perturbed values. For additional details on the parameterisation of CO_2 response in GLAM the reader is referred to Challinor and Wheeler (2008a).

Table S1 Parameterisations of CO_2 response used and changes to relevant GLAM model parameters

ID	Description	T_{fac}	E_T	T_{Tmax}	SLA_{max}
C1	No stimulation at low VPD Moderate increase in E_T	0.0	+8.8 %	–6.23 %	–3.67 %
C2	No stimulation at low VPD Large increase in E_T	0.0	+14.7 %	–6.23 %	–3.67 %
C3	Moderate stimulation at low VPD Moderate increase in E_T	0.4	+8.8 %	–6.23 %	–3.67 %
C4	Moderate stimulation at low VPD Large increase in E_T	0.4	+14.7 %	–6.23 %	–3.67 %

SI Text 2: Crop model calibration and evaluation

This section describes methods for model calibration and evaluation, and summarises results of model evaluation.

i. Model calibration: In order to calibrate GLAM, the definition of 23 site-independent (i.e. global) model parameters and 1 'local' parameter is required. The values of the 23 global parameters are constant across large and relatively uniform areas, such as those where duration requirements are known not to vary significantly. The only local parameter that needs to be calibrated is the yield gap parameter (C_{YG}), which is obtained separately for each grid cell. In this study, the domains across which 'global' parameters were defined were those of Fig. 1A. Model calibration was carried out separately for each of these zones by minimising the Root Mean Square Error (RMSE, Eq. S1) between observed and simulated yield.

$$RMSE = \sqrt{\frac{\sum_{i=1}^{n}\left(O_i - P_i\right)^2}{n}} \qquad \text{[Equation S1]}$$

where *O* and *P* refer to observed and predicted quantities of a series of *n* elements (here, n = 28 years). *RMSE* was used as it provides a complete measure of the model errors (Taylor 2001). Calibration of model parameters was then conducted as follows:

(1) First, in order to minimise the interactions between C_{YG} and all other parameters, the single grid cell with the highest yield per growing zone was selected for global parameter calibration. We assume that this single grid cell is close to the average potential on-farm yields for a large and relatively homogeneous region (i.e. the growing zone of Fig. 1A, main text), and thus is assigned a value of C_{YG} = 1.0 throughout the rest of the calibration process. This assumption was made given the high average yield levels of some grid cells per growing zone. In addition, the use of a single grid cell also provided the opportunity to evaluate the skill of the model and its global parameters in grid cells not used for global calibration.

(2) We then developed a parameter ensemble for each growing zone by performing a total of 50 parallel calibration chains. We attempted 50 chains due to the computational needs for the genotypic adaptation simulations (see main text). Each calibration chain had a different order for parameter calibration, and started at a different point of the parameter space (i.e. a different value for each of the parameters). Both the starting values for each of the 23 parameters as well as the order of parameters during calibration were chosen at random for each chain. In each chain, parameters were calibrated by iteratively testing values within known parameter ranges (Challinor et al. 2004; Ramirez-Villegas et al. 2015). As we ran 15 iterations for each chain, this

resulted in a total of 17,250 calibration runs being performed per growing zone (23 parameters x 15 iterations x 50 chains). Similar to other parameter estimation methods [e.g. Beven and Freer (2001)], this method also allows a random sampling of the parameter space, and accounts for co-variation in parameter values.

(3) Next, from all calibration runs we selected all unique parameter sets that were skilful enough and hence could be considered as 'behavioural' (Beven and Freer 2001). More specifically, from the 50 initial parameter sets that resulted from the 50 calibration chains, the single one with lowest *RMSE* ('reference') was selected and compared with the remaining 49 through a Kolmogorov-Smirnov non-parametric test. This yielded 19 parameter sets whose distribution was found statistically similar to the reference.

(4) Finally, for each chain, C_{YG} was calibrated on a grid cell basis by iteratively testing values between 0.0 and 1.0 (at steps of 0.01) that minimised the RMSE.

ii. Model evaluation: To provide a general idea of GLAM's skill across the full set of potential parameter combinations the skill of the 50 parameter ensemble members was assessed in the following ways:

(1) A Taylor diagram (Taylor 2001) was constructed to summarise the skill of all parameter ensemble members. A Taylor diagram summarises how well a model simulation matches observations in terms of correlation, *RMSE* and ratio of variances. A diagram for each characteristic (i.e. crop yield mean and standard deviation) was finally produced.

(2) The correlation coefficient and the *RMSE* were calculated for each grid cell and parameter ensemble member to produce maps showing the variation of these two metrics across the geographic and parameter space.

(3) The 28-year calibration period was split into two halves so as to cross-calibrate C_{YG}.

The performance of the 50 parameter sets is shown in the form of two Taylor diagrams (Fig. S1) for both the spatial consistency of the mean yields and of the interannual variability of yields (i.e. the standard deviation). Each dot in the figure represents a single parameter ensemble member where all the three metrics have been calculated pair-wise using the time-mean (Fig. S1A) and the time-standard deviation (Fig. S1B) of all grid cells. Blue coloured dots show the 19 parameter ensemble members that were considered to represent crop yields reliably. GLAM represented mean yields with a higher degree of accuracy as compared to interannual variations.

The spatial correlation coefficient of mean yields was in all parameter ensemble members above 0.8 (maximum r=0.98, $p\leq0.001$). The representation of standard deviations was much more limited in the model, with all parameter sets showing a spatial correlation coefficient below 0.5 (maximum r=0.45, $p\leq0.001$), and the *RMSE* of the normalised standard deviations (grey arcs concentric to the unity in the x-axis) being relatively large.

The statistical characteristics of the crop yields were, however, well captured by the crop model, particularly in the selected parameter ensemble members (blue dots that are close to the black continuous standard deviation arc in Fig. S1).

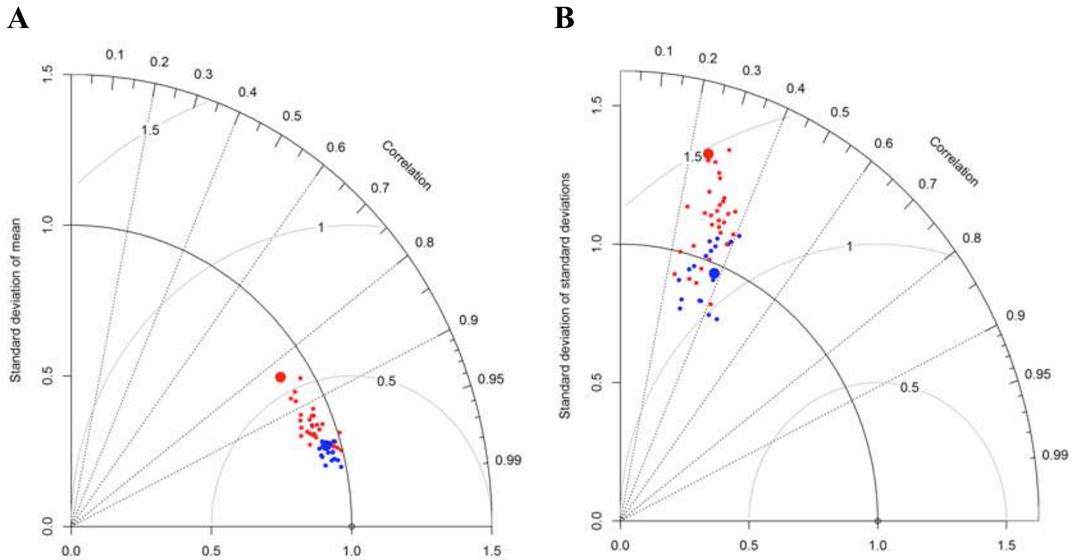

Figure S1 Taylor diagram showing the performance of the 50 parameter ensemble members in relation to the spatial variation in mean (A) and standard deviation (B) of yields. Spatial standard deviations are normalised to observed (hence the "perfect" standard deviation is the continuous black arc at 1.0 –concentric to the origin). Grey arcs concentric to 1.0 in the x-axis represent the *RMSE*. Blue and red colours indicate selected and discarded parameter ensemble members, respectively. Large filled dots indicate parameter sets shown in detail in Figure S2.

The low performance parameter ensemble member marked in Fig. S1 showed one of the lowest correlations (r=0.25 and r=0.83 for standard deviation and mean yields, respectively), a significantly higher spatial standard deviation of the yield variability (about 1.3 times higher), and the largest centred *RMSE* for both the mean and variability of yields (1.5 and 0.5, respectively) (Fig. S2). By contrast, the high performance parameter ensemble member showed a near-perfect representation of the standard deviations, a near-perfect correlation for mean yields (r=0.97, $p \leq 0.0001$) and a relatively strong correlation for yield variability (r=0.38, $p \leq 0.0001$). Most of the statistically significant correlations were found across western, northern and central-north India, where the strongest climate signals on crop yields are reported (Challinor et al. 2003).

The simulation of interannual variability was mostly in agreement with observations across western and central India (predicted σ is between 0.8-1.2 with respect to observations), but interannual variation was over-estimated in the southern zone and the east, and under-estimated in the northern India (predicted σ up to 1.5-2 times larger than observed). Crop model errors were spatially consistent across parameter sets (Fig. S3). Most of the parameter ensemble members showed mean yield prediction between +20 and –20% of observed yields in nearly 80% of the analysed areas, regardless of the parameter ensemble member. In the remainder of areas, a trend to under-estimate mean crop yields beyond -20% (nearly up to -50%) was observed.

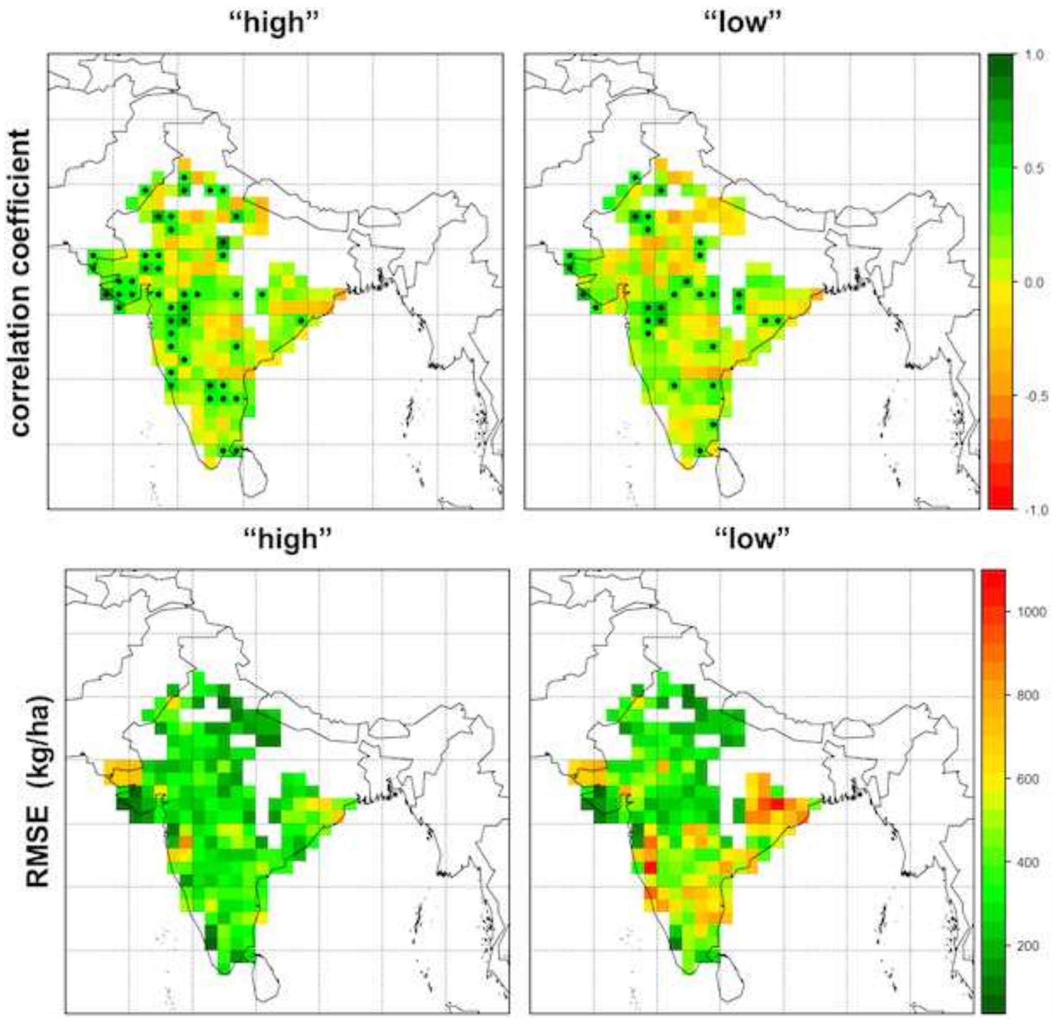

Figure S2 Spatial distribution of two crop model skill metrics for two selected parameter ensemble members (marked with large filled circles in Fig. S1). The captions “high” and “low” indicate that the parameter ensemble members are high- and low-skill, respectively (differentiated by blue and red colours in Fig. S1). Filled dots in the correlation coefficient maps indicate statistically significant correlations ($p \leq 0.1$).

The values of the yield gap parameter varied only slightly from one period to the other, particularly for the most skilful parameter sets. The areas where the most significant changes in C_{YG} occurred are located towards the very north of India. In these areas, C_{YG} increased by 30-40 % between the two periods. A PDF of the spearman rank correlation (*rho*) between the two time periods showed that the relationship is strong and statistically significant (Fig. S4). In particular, for the selected parameter sets (blue line in Fig. S4), the values of *rho* were high (0.75-0.9). Differences in the values of the C_{YG} through time can be attributed to changes in the main drivers of crop production through time (i.e. from water- to radiation-limited), noise in the yield time series, the assumption that the technology trend is linear [whereas it could in some cases be non-linear, see e.g. Baigorria et al. (2010)], the fact that this area is largely irrigated (Mehrotra 2011), or to structural errors in the crop model.

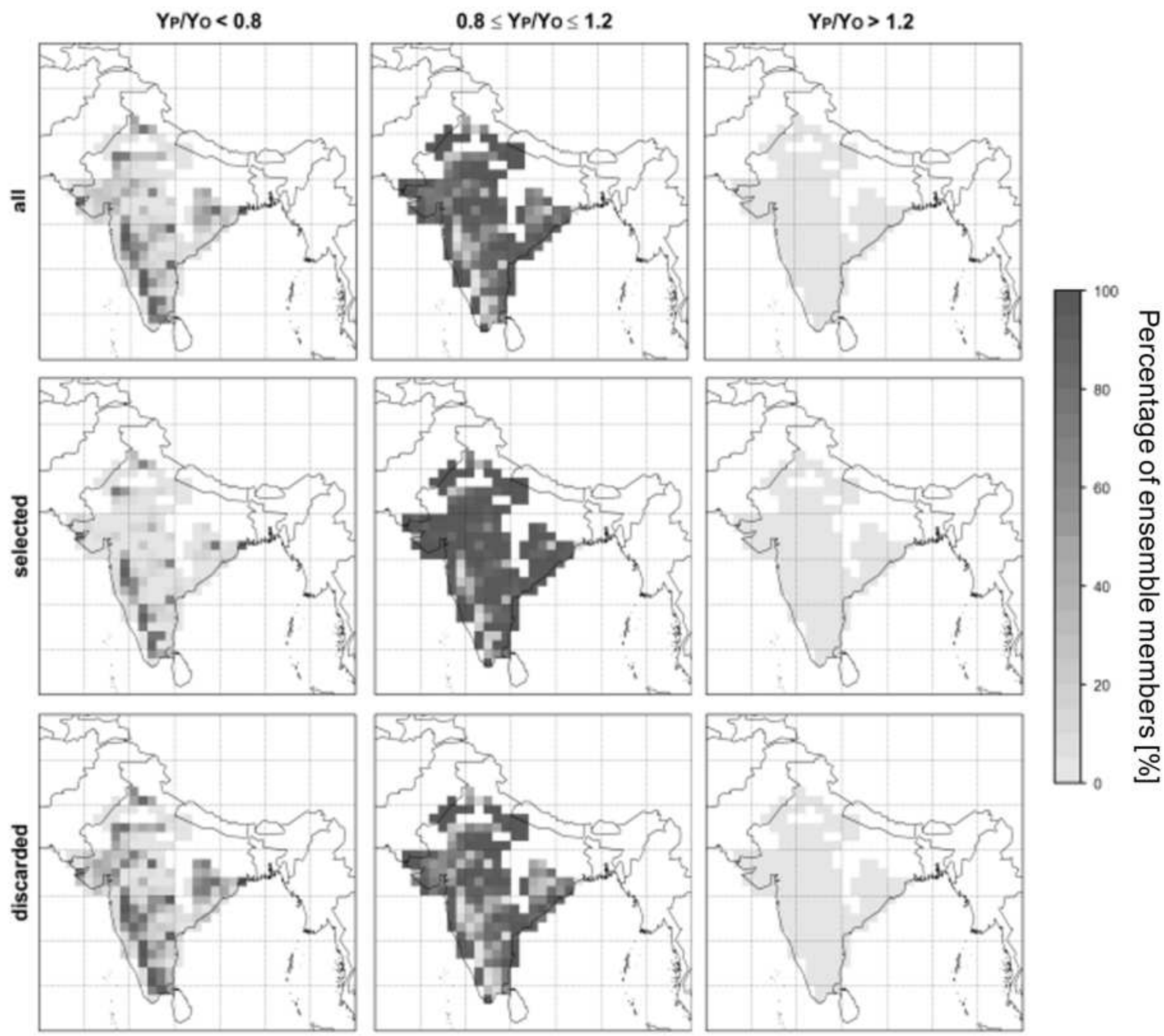

Figure S3 Percent of parameter ensemble members for which the normalised-by-observed predicted mean yields falls in each of three categories: underestimating (predicted yield [Y_P] by observed yield [Y_O] < 0.8; i.e. $Y_P/Y_O < 0.8$), normal (Y_P/Y_O between 0.8 and 1.2), and overestimating ($Y_P/Y_O > 1.2$). Parameter ensemble members are classified in three categories: all 50 members, selected 19 members and 31 discarded members (shown in different rows).

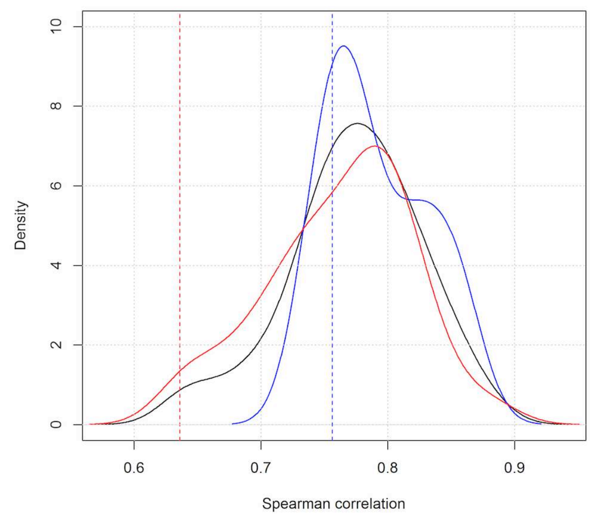

Figure S4 Probability density function of the Spearman rank correlation between the two yield gap parameter (C_{YG}) values (C_{YG1}: 1966-1979 and C_{YG2}: 1980-1993) for all parameter ensemble members (n=50, black line), selected parameter ensemble members (n=19, blue line) and discarded parameter ensemble members (n=31, red line). Each PDF curve is calculated using the n parameter sets of each category. For each parameter set a single value of the Spearman correlation (*rho*) was computed using 195 pairs of [C_{YG1}, C_{YG2}] values, each corresponding to a grid cell of the analysis domain. Dashed vertical lines show the low (red) and high (blue) parameter sets indicated as large dots in Fig. S1).

SI Text 3: Changes in groundnut productivity under no-adaptation scenarios

Baseline values and projected changes in mean yields are shown in Figure S5. There were significant yield increases projected across the major growing areas in the west of India (Gujarat state). Yield losses below 20 % were found highly unlikely across the entire region. There was significant uncertainty as per the direction of the change in central India, although the probability of a negative impact was generally larger than that of a positive impact. Conversely, in eastern India, yield gains were found more often in the ensemble of model runs than those of negative impacts. These results broadly agree with those of refs. (Challinor and Wheeler 2008b; 2009), which projected yield losses in central India, and yield gains in north-west and western India. The choice of how GCM outputs are bias-corrected did not affect the direction of change but did so for the extent of the change (Figure S5D, E, F).

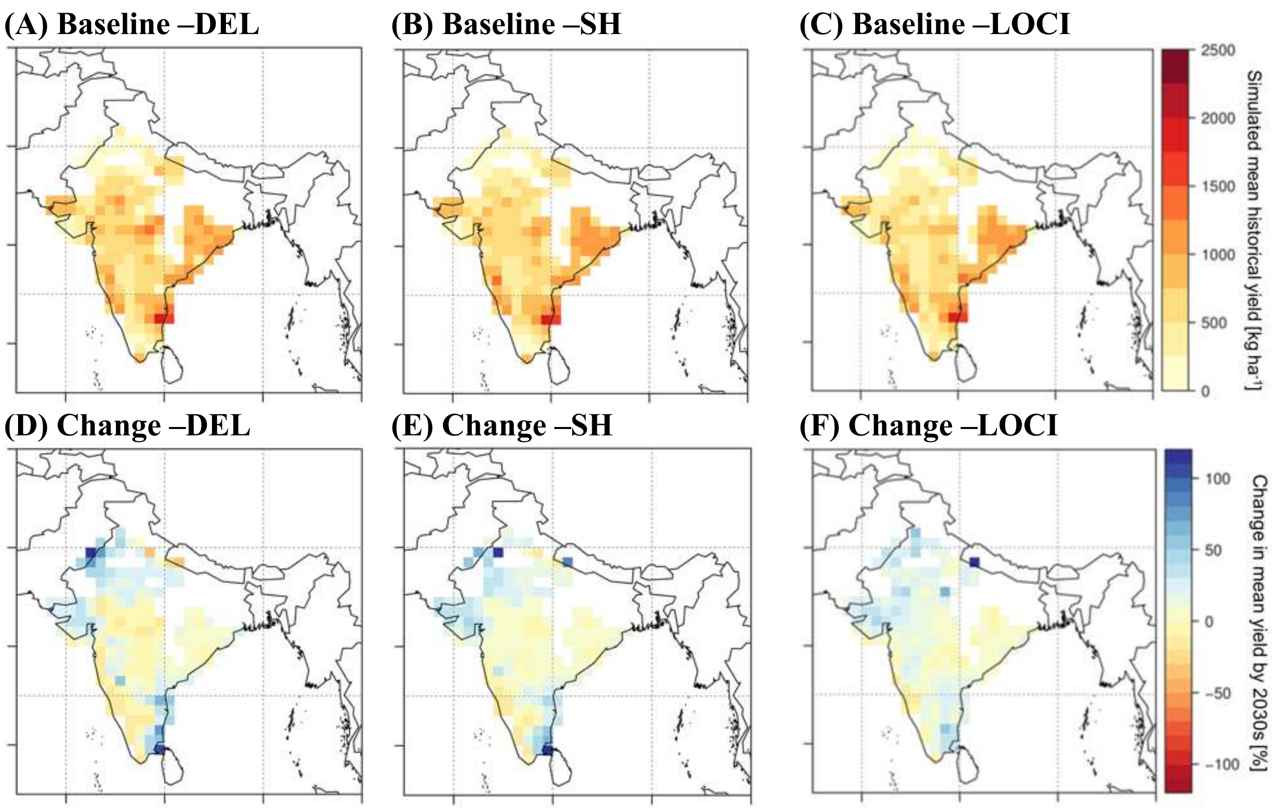

Figure S5 Baseline (A, B, C) and future projected changes (D, E, F) in mean crop yield for (A, E) simulations using DEL-corrected GCM outputs (A, D), SH-corrected GCM outputs (B, E), and LOCI-corrected GCM outputs (C, F). Values shown are means across all simulations (i.e. GLAM parameter ensemble members, GCMs, CO_2 response parameterisations) for each bias correction method.

Projections of changes in yield variability (*CV*) showed less consistent patterns (Fig. S6). In general, the eastern part of the peninsular zone showed decreases in yield *CV*. Minor decreases (0-5 %) were observed in western and central India. Relative changes in yield variability in northern India varied substantially between LOCI and the other two input types (SH and DEL). Since in LOCI temperature bias is not corrected, this suggested that temperature bias played an important role in the changes in interannual yield variability in this region.

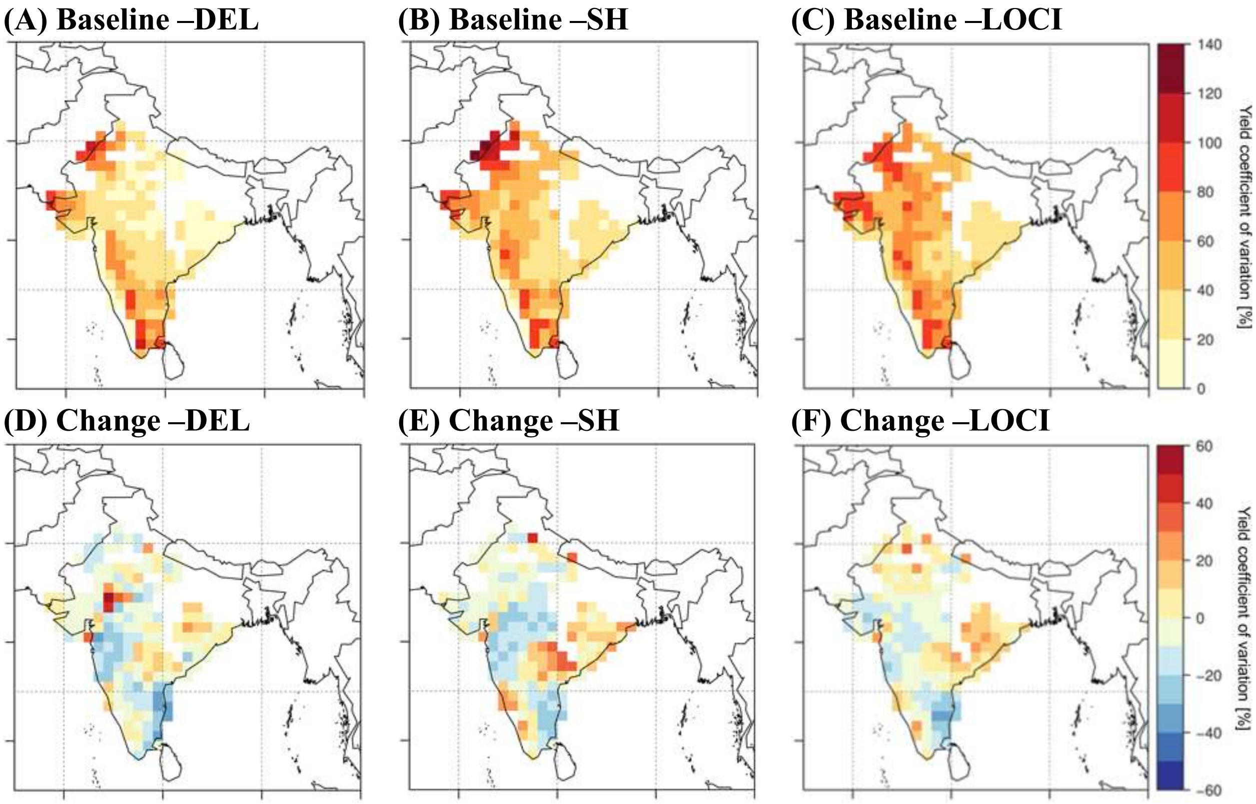

Figure S6 Baseline (A, B, C) and future (2030s) projected changes (D, E, F) in crop yield variability (i.e. coefficient of variation) for (A, E) simulations using DEL-corrected GCM outputs (A, D), SH-corrected GCM outputs (B, E), and LOCI-corrected GCM outputs (C, F). Values shown are means across all simulations (i.e. GLAM ensemble members, GCMs, CO_2 response parameterisations) for each bias correction method.

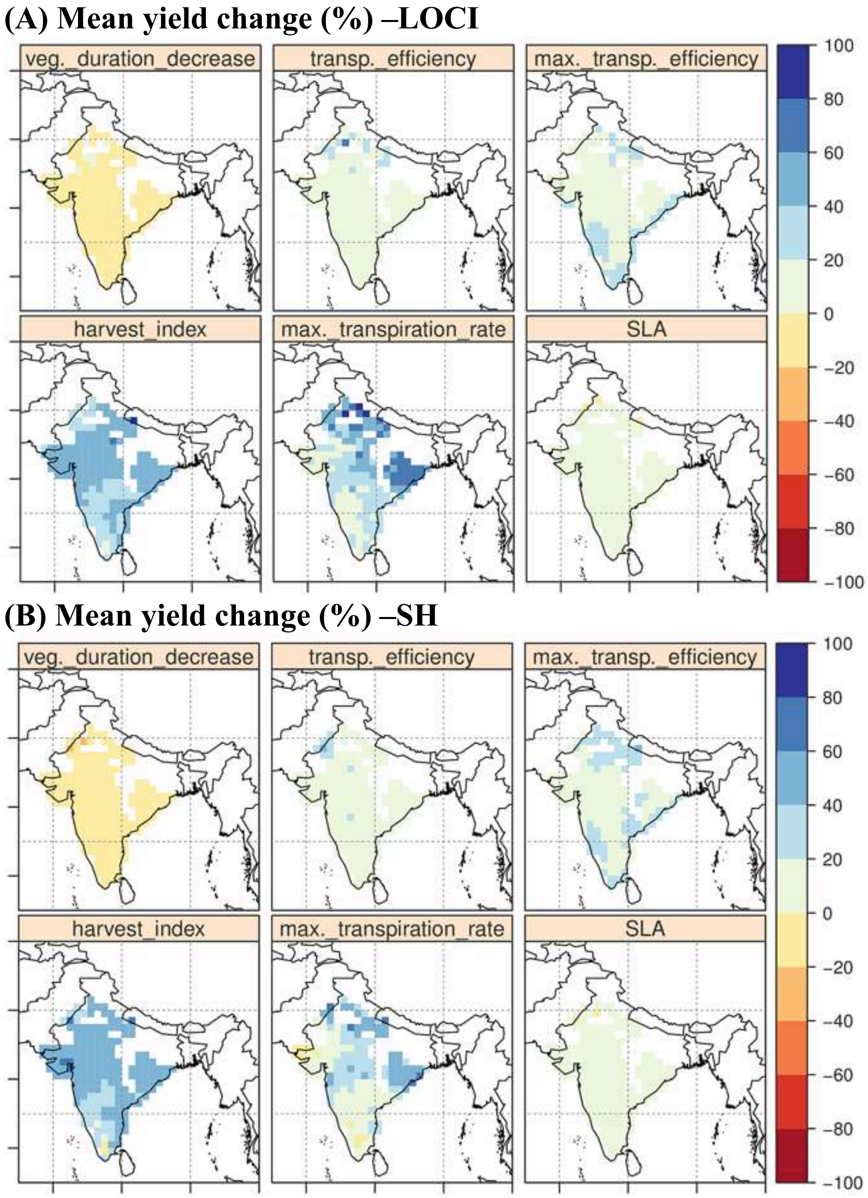

Figure S7 Projected mean yield changes by 2030s as a result of crop improvement related to drought scape and water use efficiency, expressed as percentage variation from no-adaptation simulations. Shown are the ensemble mean results of A-LOCI (A) and A-SH (B) simulations for each of the genotypic properties. Model parameters are as follows: decrease in thermal time from sowing to flowering (t_{TT0}), increase in transpiration efficiency (T_E), increase in maximum transpiration efficiency ($E_{TN,max}$), increase in rate of harvest index ($\partial H_I/\partial t$), increase in maximum transpiration rate (T_{Tmax}), and increase in specific leaf area (SLA_{max}).

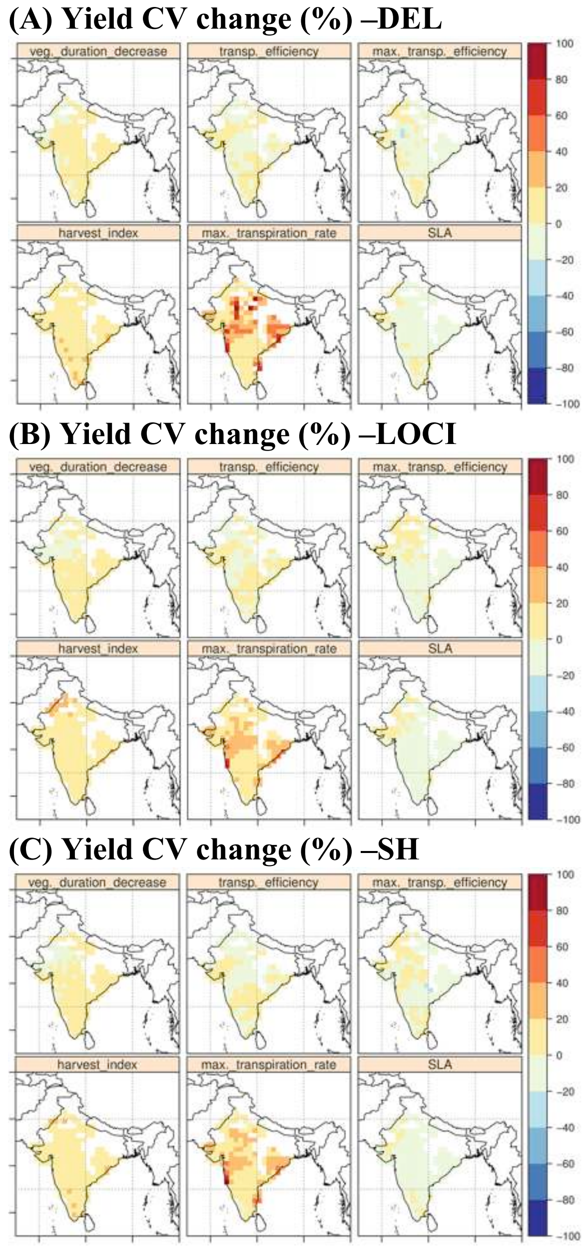

Figure S8 Projected yield variability (CV) changes by 2030s as a result of crop improvement related to drought scape and water use efficiency for (A) A-DEL, (B) A-LOCI and (C) A-SH simulations, expressed as percentage variation from no-adaptation simulations. Associated model parameters are as follows: decrease in vegetative duration (t_{TT0}), increase in transpiration efficiency (T_E), increase in maximum transpiration efficiency (E_{TNmax}), increase in rate of harvest index ($\partial H_I/\partial t$), increase in maximum transpiration rate (T_{Tmax}), and increase in specific leaf area (SLA_{max}).

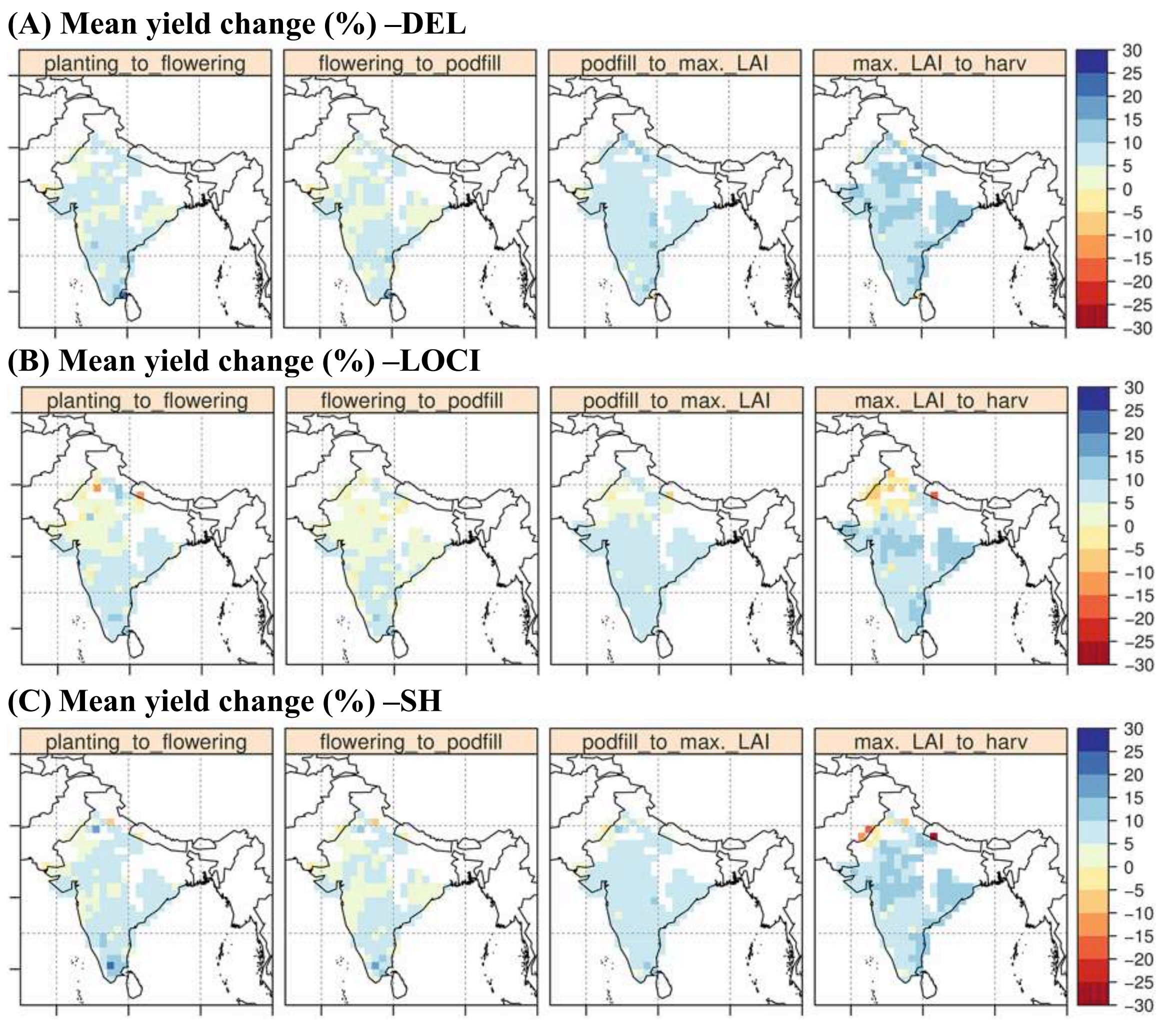

Figure S9 Projected mean yield changes by 2030s as a result of increased crop duration. Shown are the ensemble mean results of A-DEL (A), A-LOCI (B) and A-SH (C) simulations for each of the genotypic properties, expressed as percentage change from no-adaptation simulations. Associated GLAM model parameters are as follows: increase in thermal time from sowing to flowering (t_{TT0}), increase thermal requirement for flowering to start of pod-filling (t_{TT1}), increase in thermal time from start of pod-filling to maximum leaf area index (t_{TT2}), increase in thermal time from maximum LAI to physiological maturity (t_{TT3}).

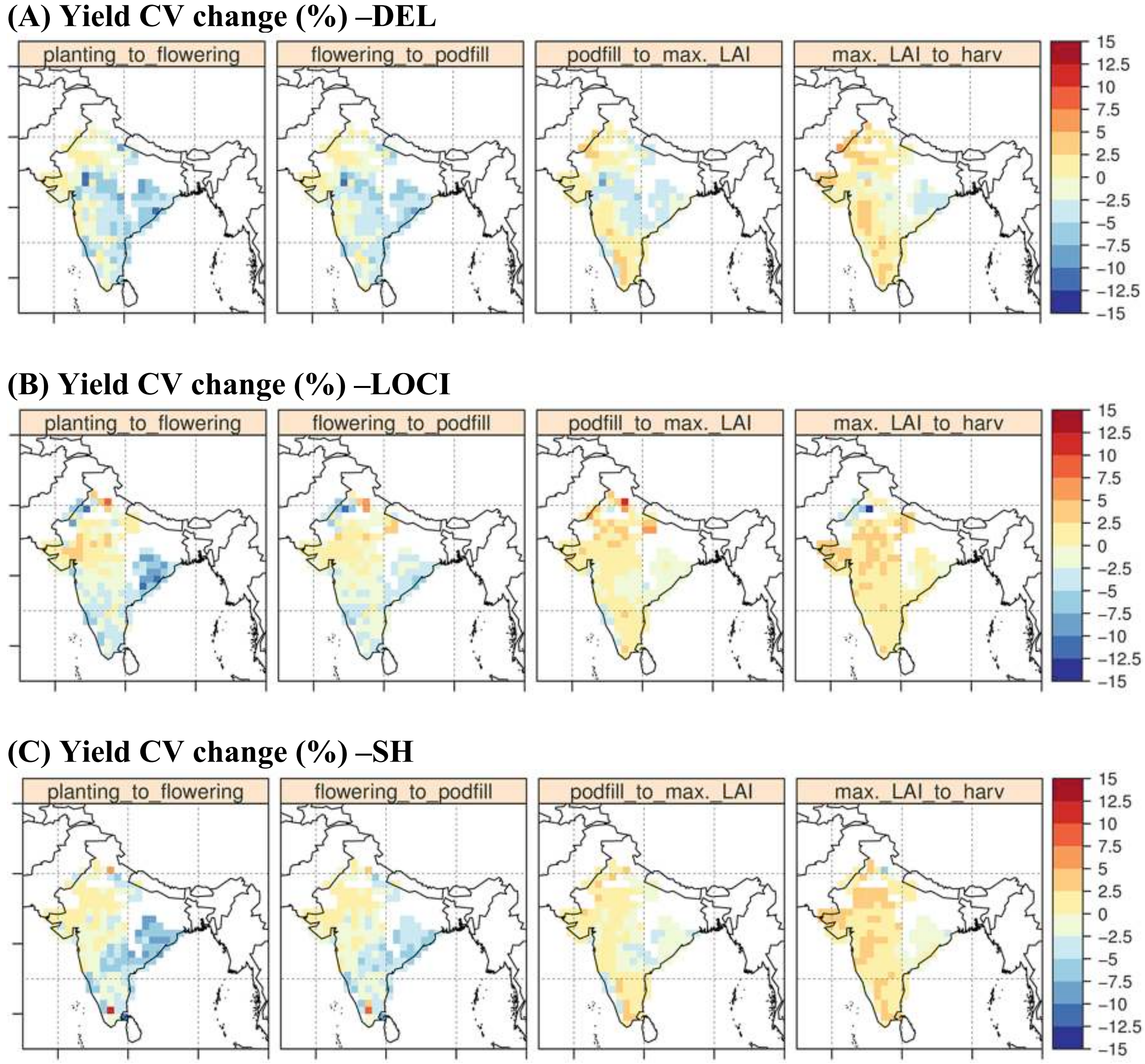

Figure S10 Projected yield variability (*CV*) changes by 2030s as a result of increased crop duration, expressed as percentage change from no-adaptation simulations. Shown are the ensemble mean results of A-DEL (A), A-LOCI (B) and A-SH (C) simulations for each of the genotypic properties. Associated GLAM model parameters are as follows: increase in thermal time from planting to flowering (t_{TT0}), increase thermal requirement for flowering to start of pod-filling (t_{TT1}), increase in thermal time from start of pod-filling to maximum leaf area index (t_{TT2}), increase in thermal time from maximum LAI to physiological maturity (t_{TT3}).

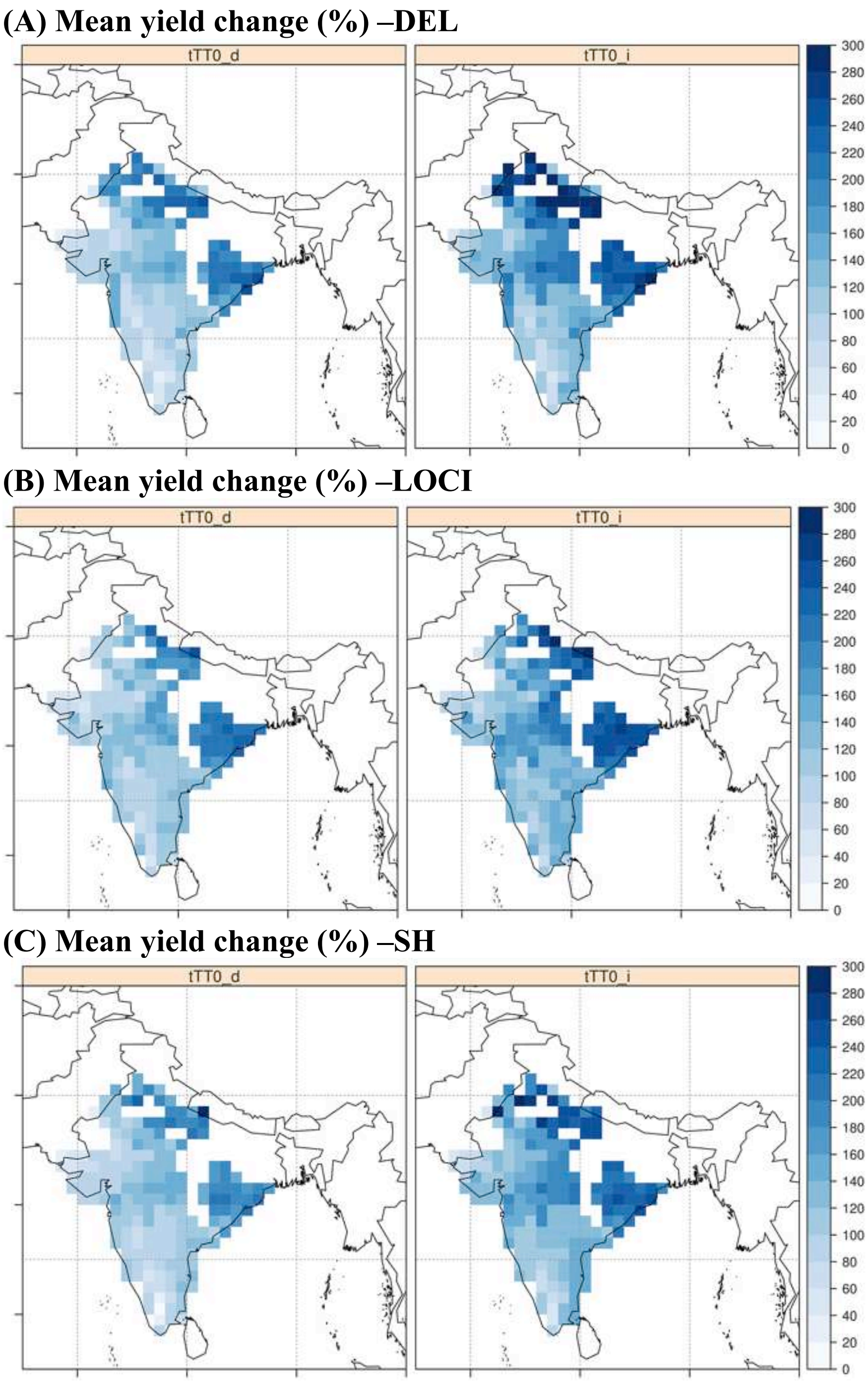

Figure S11 Projected crop yield mean changes by 2030s as a result of combined-trait improvement scenarios, expressed as percentage change from no-adaptation simulations. Shown are the ensemble mean results of A-DEL (A), A-LOCI (B) and A-SH (C) simulations for each genotypic improvement scenario. Scenario "tTT0_d" refers to increases in T_E, $E_{TN,\, max}$, T_{Tmax}, SLA_{max}, $\partial H_I/\partial t$, t_{TT1}, t_{TT2}, and t_{TT3} combined with decreases in t_{TT0}, whereas scenario "tTT0_i" refers to increases in the same genotypic properties combined with increases in t_{TT0}.

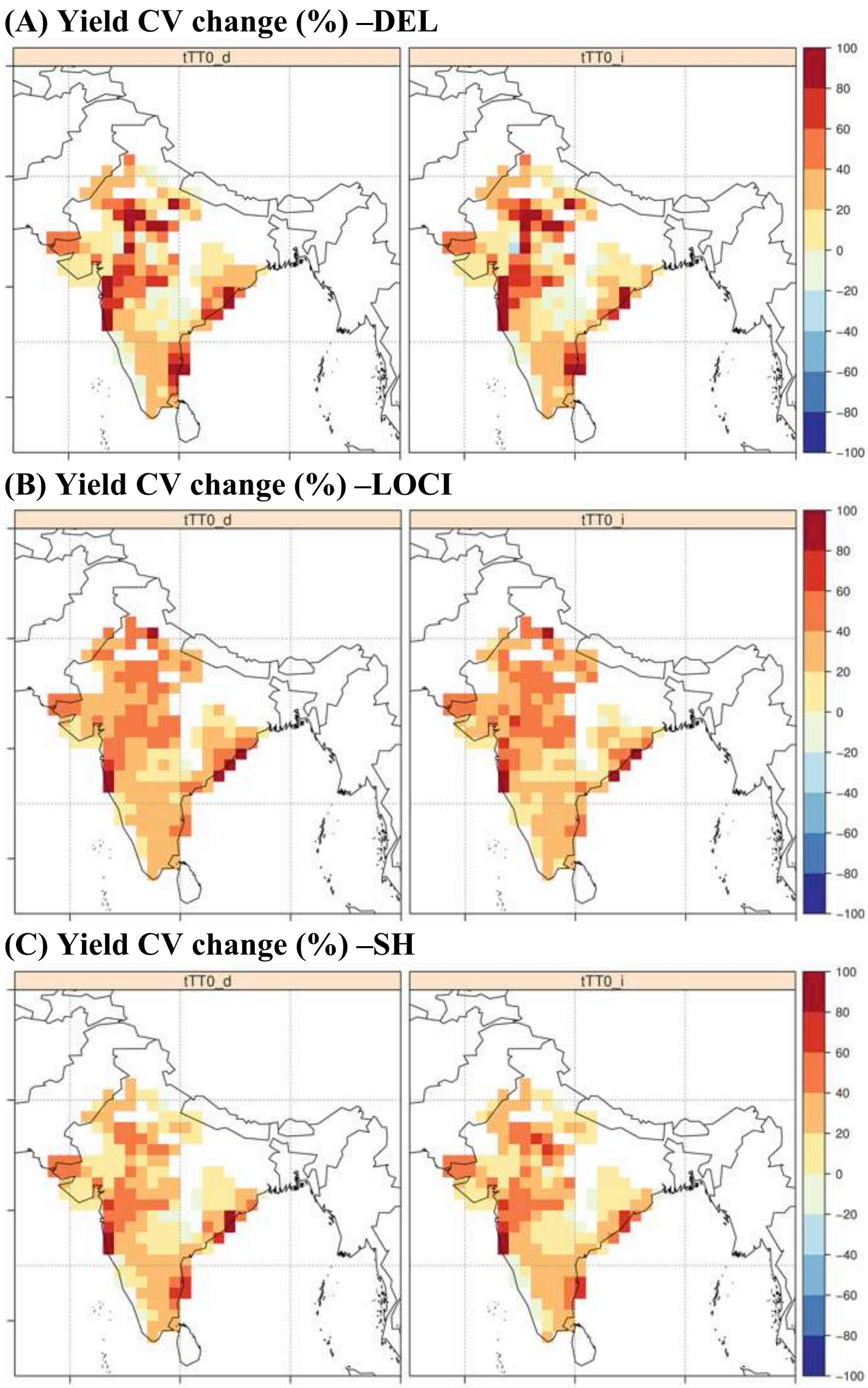

Figure S12 Projected crop yield variability (CV) changes by 2030s as a result of combined-trait improvement scenarios for (A) A-DEL, (B) A-LOCI and (C) A-SH simulations, expressed as percentage change from no-adaptation simulations. Scenario "tTT0_d" refers to increases in T_E, $E_{TN,\ max}$, T_{Tmax}, SLA_{max}, $\partial H_I/\partial t$, t_{TT1}, t_{TT2}, and t_{TT3} combined with decreases in t_{TT0}, whereas scenario "tTT0_i" refers to increases in the same genotypic properties combined with increases in t_{TT0}.

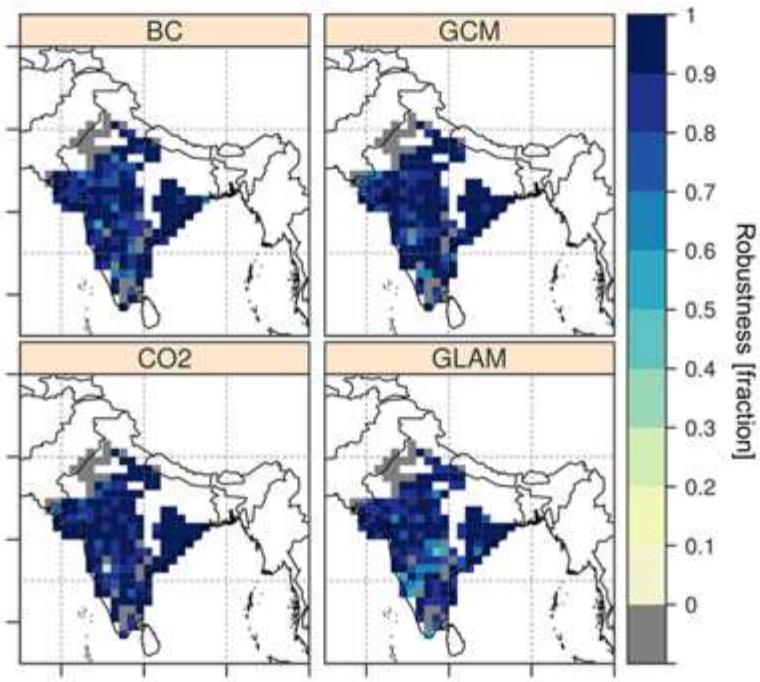

Figure S13 Robustness (R, fraction) of model projections of adaptation. Maps show robustness calculated using simulations pooled by each of the modelling choices. BC refers to bias correction method (2 ensemble members), GCM refers to choice of global climate model (13 ensemble members), CO2 refers to parameterisations of CO_2 response (4 ensemble members) and GLAM refers to choice of parameter set. Grey areas all have $R<0$, indicating poor model robustness.

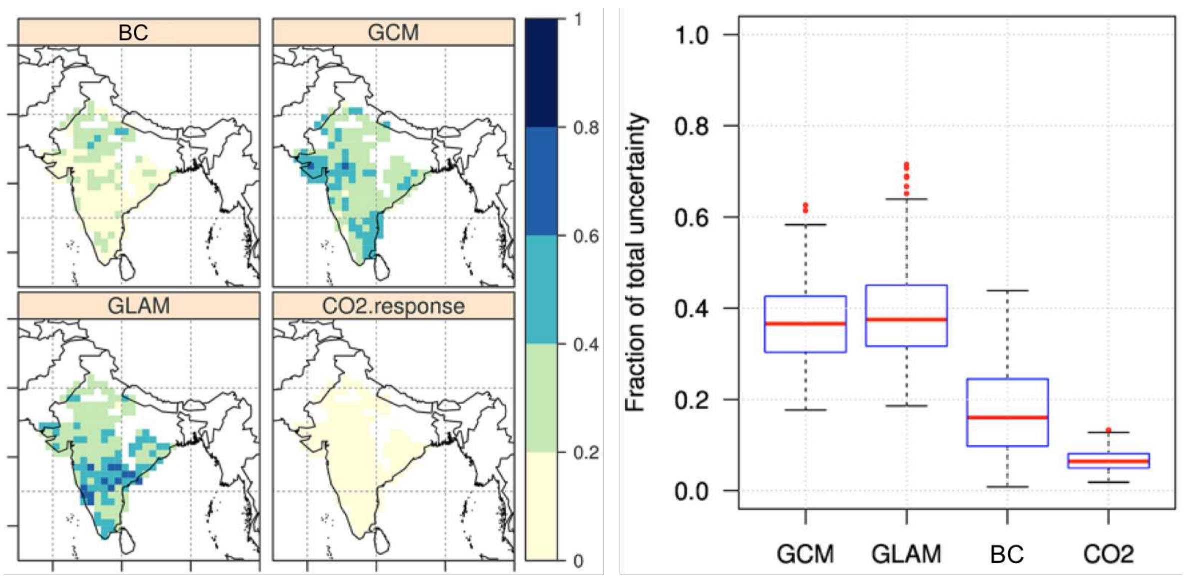

Figure S14 Relative contribution of different sources to total yield uncertainty in genotypic adaptation simulations. Maps show the geographic variation of importance in different sources, whereas the boxplots show the general trend across the country (spread being spatial variation). Thick horizontal red line is the median, blue boxes mark the 25 and 75 % of the data and black whiskers extend to 5 and 95 % of the data. BC uncertainty refers to the choice bias correction method.

Table S2 CMIP5 GCMs used in the study and main characteristics

Model name[1]	NC[2]	HRx[3]	NR[2]	HRy[3]	Calendar[4]
BCC-CSM1.1	128	2.8125	64	2.8125	365
BNU-ESM	128	2.8125	44	4.0909	365
CCCMA-CanESM2	128	2.8125	64	2.8125	365
CNRM-CM5	256	1.4063	128	1.4063	366
CSIRO-Mk3.6.0	192	1.875	96	1.875	365
INM-CM4	180	2.000	120	1.500	365
IPSL-CM5a-LR	96	3.750	96	1.875	365
IPSL-CM5b-LR	96	3.750	96	1.875	365
MOHC-HadGEM2-CC	192	1.875	145	1.2414	360
MOHC-HadGEM2-ES	192	1.875	145	1.2414	360
MPI-ESM-LR	192	1.875	96	1.875	366
MPI-ESM-MR	192	1.875	96	1.875	366
MRI-CGCM3	320	1.125	160	1.125	366

[1] In all cases only one ensemble member was used (r1i1p1) as described in ref. (2012).
[2] NC and NR Number of columns (NC) and rows (NR) in the climate grid.
[3] HRx and HRy refer to horizontal resolution in the *x*-axis (longitude, HRx) and the *y*-axis (latitude, HRy), in decimal degree.
[4] Calendar type refers to that used in the climate model run: 365 is a calendar without leap years, 366 is the standard Gregorian calendar (with leap year), and 360 refers to the calendar in which all months have 30 days only used by the UK MetOffice climate models.

Table S3 Summary of studies of genotypic adaptation and ideotype design

Study	Region	Genotypic property	Crop response
Challinor *et al.* (2009)	India	Total thermal requirement	Increases in thermal requirement are needed between 20-30 % to counter yield loss by 2100
Challinor *et al.* (2007)	India	Tolerance to high temperature	Increased heat stress tolerance reduces yield loss by 50-80 % by 2100
		Change in optimal temperature for development	No beneficial effect observed with increases in T_{opt} from 28 ºC to 36 ºC
Suriharn *et al.* (2011)	Thailand	Thermal requirement during vegetative phase	Yield gain when vegetative duration was decreased
		Thermal requirement during pod-filling phase	Yield gain when pod-filling duration was increased
		Thermal requirement during flowering to max. LAI	Increases are crucial for achieving high LAI
		Maximum leaf size	Minimal effect due to increased light competition
		Specific leaf area	Increases in yield, but countered increases in maximum photosynthetic rate
		Maximum rate of photosynthesis	Increase of 7 % in $P_{N, max}$ increased yield by up to 150 %
		Partitioning to seed	Increases of up to 10 % boosted yields by 200 %
Singh *et al.* (2012, 2013)	India West Africa	Thermal requirement from emergence to flowering	Increases produced little gain or yield loss
		Thermal requirement during pod-filling phase	Increase of 10 % produced yield gains of 2.5 - 8 %
		Maximum leaf size	Little or no yield gain
		Specific leaf area	Gains restricted to low temperature areas, where VPD is low
		Maximum rate of photosynthesis	Gains between 4-5 % at all locations
		Seed filling duration	Gains between 3-5 % at all locations
		Nitrogen mobilisation rate	Small yield gains between 1-2.5 % at all locations
		Pod adding duration	Moderate (2-5 %) yield gain restricted to warm sites
		Fraction assimilate partitioned to seed	Increased yield by up to 5 % at all locations
		Fraction assimilate partitioned to roots	Detrimental to yield
		Root biomass across soil profile	Little gain or yield loss
		Velocity of extraction front	Little to no yield gain
		Temperature tolerance for pod-set, partitioning to pods and individual seed growth	Large yield gains (8-13 %) in warm areas

Supplementary references

Baigorria GA, Chelliah M, Mo KC, et al. (2010) Forecasting Cotton Yield in the Southeastern United States using Coupled Global Circulation Models. Agron J 102:187–196. doi: 10.2134/agronj2009.0201

Beven K, Freer J (2001) Equifinality , data assimilation , and uncertainty estimation in mechanistic modelling of complex environmental systems using the GLUE methodology. J Hydrol 249:11–29.

Challinor A, Wheeler T, Hemming D, Upadhyaya H (2009) Ensemble yield simulations: crop and climate uncertainties, sensitivity to temperature and genotypic adaptation to climate change. Clim Res 38:117–127. doi: 10.3354/cr00779

Challinor AJ, Slingo JM, Wheeler TR, et al. (2003) Toward a Combined Seasonal Weather and Crop Productivity Forecasting System: Determination of the Working Spatial Scale. J Appl Meteorol 42:175–192. doi: doi:10.1175/1520-0450(2003)042<0175:TACSWA>2.0.CO;2

Challinor AJ, Wheeler TR (2008a) Use of a crop model ensemble to quantify CO2 stimulation of water-stressed and well-watered crops. Agric For Meteorol 148:1062–1077. doi: DOI: 10.1016/j.agrformet.2008.02.006

Challinor AJ, Wheeler TR (2008b) Crop yield reduction in the tropics under climate change: Processes and uncertainties. Agric For Meteorol 148:343–356. doi: DOI: 10.1016/j.agrformet.2007.09.015

Challinor AJ, Wheeler TR, Craufurd PQ, et al. (2004) Design and optimisation of a large-area process-based model for annual crops. Agric For Meteorol 124:99–120. doi: DOI: 10.1016/j.agrformet.2004.01.002

Chen JJ, Sung JM (1990) Gas Exchange Rate and Yield Responses of Virginia-type Peanut to Carbon Dioxide Enrichment. Crop Sci 30:1085–1089. doi: 10.2135/cropsci1990.0011183X003000050025x

Clifford SC, Stronach IM, Black CR, et al. (2000) Effects of elevated CO2, drought and temperature on the water relations and gas exchange of groundnut (Arachis hypogaea) stands grown in controlled environment glasshouses. Physiol Plant 110:78–88. doi: 10.1034/j.1399-3054.2000.110111.x

Jones JW, Hoogenboom G, Porter CH, et al. (2003) The DSSAT cropping system model. Eur J Agron 18:235–265. doi: Doi: 10.1016/s1161-0301(02)00107-7

Keating BA, Carberry PS, Hammer GL, et al. (2003) An overview of APSIM, a model designed for farming systems simulation. Eur J Agron 18:267–288. doi: 10.1016/s1161-0301(02)00108-9

Leakey ADB, Ainsworth EA, Bernacchi CJ, et al. (2009) Elevated CO2 effects on plant carbon, nitrogen, and water relations: six important lessons from FACE. J Exp Bot 60:2859–2876. doi: 10.1093/jxb/erp096

Long SP, Ainsworth EA, Leakey ADB, et al. (2006) Food for Thought: Lower-Than-Expected Crop Yield Stimulation with Rising CO2 Concentrations. Science (80-) 312:1918–1921. doi: 10.1126/science.1114722

Mehrotra N (2011) Groundnut. Department of Economic Analysis and Research, National Bank for Agriculture and Rural Development, Mumbai, India

Ramirez-Villegas J, Koehler A-K, Challinor AJ (2015) Assessing uncertainty and complexity in regional-scale crop model simulations. Eur J Agron. doi: 10.1016/j.eja.2015.11.021

Schmidt GA, Ruedy R, Hansen JE, et al. (2006) Present-Day Atmospheric Simulations Using GISS ModelE: Comparison to In Situ, Satellite, and Reanalysis Data. J Clim 19:153–192. doi: 10.1175/jcli3612.1

Seeni S, Gnanam A (1982) Carbon Assimilation in Photoheterotrophic Cells of Peanut (Arachis hypogaea L.) Grown in Still Nutrient Medium. Plant Physiol 70:823–826. doi: 10.1104/pp.70.3.823

Stanciel K, Mortley DG, Hileman DR, et al. (2000) Growth, Pod, and Seed Yield, and Gas Exchange of Hydroponically Grown Peanut in Response to CO2 Enrichment. HortScience 35:49–52.

Taylor KE (2001) Summarizing multiple aspects of model performance in a single diagram. J Geophys Res 106:7183–7192. doi: 10.1029/2000jd900719

Taylor KE, Stouffer RJ, Meehl GA (2012) An overview of CMIP5 and the Experiment Design. Bull Am Meteorol Soc 1–39. doi: 10.1175/BAMS-D-11-00094.1

Tubiello FN, Ewert F (2002) Simulating the effects of elevated CO2 on crops: approaches and applications for climate change. Eur J Agron 18:57–74. doi: 10.1016/s1161-0301(02)00097-7

Vara Prasad P V, Boote KJ, Hartwell Allen L, Thomas JMG (2003) Super-optimal temperatures are detrimental to peanut (Arachis hypogaea L.) reproductive processes and yield at both ambient and elevated carbon dioxide. Glob Chang Biol 9:1775–1787. doi: 10.1046/j.1365-2486.2003.00708.x